Modulation Transfer Function of a Selenium-Based Digital Mammography System

M. Hoheisel, L. Bätz, T. Mertelmeier, J. Giersch, and A. Korn

***Abstract*—Digital mammography systems with detectors based on amorphous selenium exhibit outstanding spatial resolution characterized by the modulation transfer function (MTF). We measured the detector behavior of the Siemens Mammomat Novation^{DR} with 70 μm pixel pitch and compared the results to analytical evaluations based on Monte Carlo simulations. Experimentally, the MTF of the mammography system is obtained from the images of a lead bar pattern or an edge phantom using different X-ray spectra. The simulations take into account all relevant X-ray interactions in the selenium layer. The resulting line-spread function is transformed to the MTF. Even at the Nyquist frequency (i.e., 7.14 mm^{-1}), the measured MTF is well above 45% and thus fairly close to its theoretical limit (64%). The MTF shows a few percentage points of low-frequency drop, which can be explained in part by the presence of scattered radiation. The simulations allow the features observed to be explained. The detector investigated provides excellent spatial resolution and appears well suited for high-end mammography.**

***Index Terms*—Medical imaging, Monte Carlo simulations, scattering, X-ray detector.**

I. Introduction

DIGITAL mammography systems with detectors based on amorphous selenium are currently being introduced [1], [2]. Mammography systems with a detector combining a scintillator and a photodiode matrix are already in the market, e.g., the systems of G. E. Medical Systems [3] and Fischer [4]. Mammography detectors applying selenium as a direct converter may be advantageous compared to those using a scintillator because of their outstanding spatial resolution characterized by the modulation transfer function (MTF), in particular for the detection and diagnosis of microcalcifications.

The MTF can be analyzed by numerical procedures based on various kinds of images. An image of a test object, i.e., a bar pattern grid [5], [6], a totally absorbing edge [7], or a slit, is recorded and the resulting modulation, edge spread function, or line spread function, respectively, is derived from the image. The presampled MTF can be calculated from either one of these quantities [8]. To understand the underlying processes, we also studied all relevant X-ray interactions (absorption, generation of secondary quanta, scattering) by Monte Carlo simulations.

Special attention was placed on backscattering by the different components of the detector in order to explain the observed low-frequency drop in the MTF. The influence of the substrate material on the MTF at energies as high as 120 keV had been investigated by Flynn *et al.* [9].

TABLE I
X-Ray Spectra

Anode material	Prefilter		Additional filter		Tube voltage
	Material	Thickness	Material	Thickness	
Mo	Mo	30 μm	No additional filter		23 kV
W	Rh	50 μm	Al	2 mm	28 kV
W	Rh	50 μm	Al	2 mm	35 kV
W	Rh	50 μm	PMMA	40 mm	28 kV

II. Simulations

The signal-generating processes have been studied by Monte Carlo simulations [10] using the program ROSI (Roentgen Simulation) [11] and applying a set of realistic X-ray spectra for mammography (Table I). The additional filters are placed as close to the tube as possible to avoid the effect of extra scatter.

The first simulation step is the X-ray interaction of the incident radiation with the absorber. Quanta can be elastically scattered (Rayleigh scattering), inelastically scattered (Compton scattering) where they loose energy and fast electrons are created, or completely absorbed by a photoelectric process where fluorescence quanta as well as fast electrons are generated. The secondary quanta travel a certain distance and either finally leave the absorber or interact in a consecutive process. Thus, the X-ray absorption process is distributed in space.

The second simulation step is the energy loss of the fast electrons. They can be scattered either elastically or inelastically. In the latter process, multiple electron-hole pairs are excited. Thus, electron energy loss is also a process, which leads to signal sources distributed in space.

In the case of a directly absorbing semiconductor an electrical drift field collects the excited charge carriers. Moreover, carrier diffusion again tends to spread out the signal in space. The ratio of diffusion length to drift length is relevant to describe how the signal is blurred by charge transport.

The electrical field of 10 V/μm applied in the selenium detector with 70 μm pixel pitch proved to be more than high enough to prevent MTF deterioration. Moreover, the signal is integrated over the active pixel area. The upper limit for the MTF is defined by assuming that the pixel aperture constitutes the only blur mechanism. It is quantitatively determined as a

Manuscript received November 8, 2004; revised March 16, 2006.

M. Hoheisel is with Siemens AG Medical Solutions, D-91301 Forchheim, Germany (e-mail: martin.hoheisel@siemens.com).

L. Bätz is with Siemens AG Medical Solutions, D-91052 Erlangen, Germany (+49-9131-84-6411, e-mail: lothar.baetz@siemens.com).

T. Mertelmeier is with Siemens AG Medical Solutions, D-91052 Erlangen, Germany (e-mail: thomas.mertelmeier@siemens.com).

J. Giersch was with Physics Institute 4, University Erlangen-Nürnberg, D-91052 Erlangen, Germany. He is now with Ludwig-Maximilian-University Munich, 80799 München, Germany.

A. Korn is with Physics Institute 4, University Erlangen-Nürnberg, D-91052 Erlangen, Germany (e-mail: alexander.korn@physik.stud.uni-erlangen.de).

Digital Object Identifier 10.1109/TNS.2006.874953

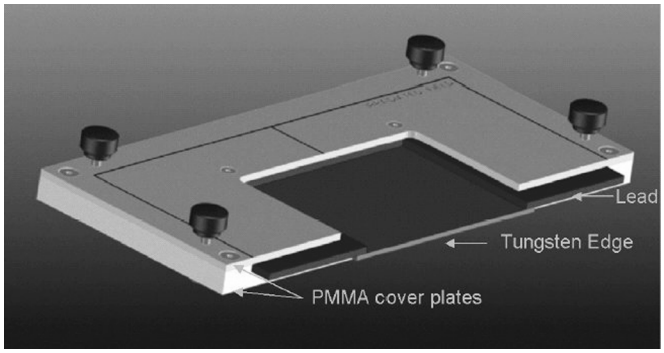

Fig. 1. A 2 mm thick tungsten edge phantom produced by Scanditronix / Wellhöfer (Schwarzenbruck, Germany).

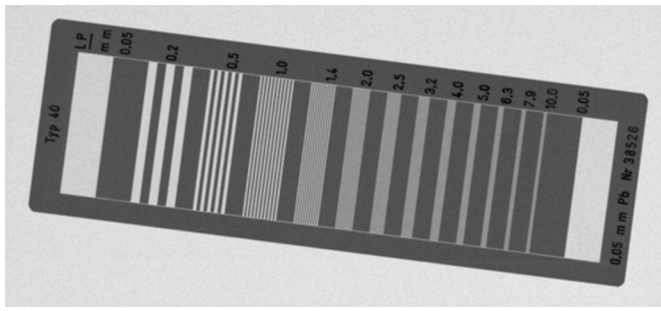

Fig. 2. Lead bar pattern type "40" produced by Hüttner (Heroldsbach, Germany). Spatial frequencies cover the range from 0.05 mm^{-1} to 10 mm^{-1}.

function of spatial frequency f and pixel aperture a by the sinc function being defined as

$$\sin c(x) = \frac{\sin(\pi x)}{\pi x} \tag{1}$$

which would describe the MTF of an ideal detector in one dimension related to an orientation in the spatial frequency plane parallel to one of the pixel lattice directions

$$\mathrm{MTF_{ideal,\,parallel}(f)} = \mathrm{sin\,c(af)}. \tag{2}$$

The idealized MTF in diagonal direction [12] for a square pixel can be derived from the two-dimensional MTF

$$\mathrm{MTF\,(f_x,\,f_y)} = \mathrm{sin\,c\,(af_x)\,sin\,c\,(af_y)} \tag{3}$$

and is given by

$$\mathrm{MTF_{ideal,\,diagonal}}(f) = \mathrm{sin\,c^2}\left(\frac{\mathrm{af}}{\sqrt{2}}\right). \tag{4}$$

The curves in this work are calculated up to the frequency where the sinc function equals zero. The values above the Nyquist frequency (i.e. 7.14 mm^{-1}), however, do not contribute to the detective quantum efficiency (DQE) of the detector.

The detector has a 250 μm thick Se absorber on an a-Si thin-film transistor matrix deposited on a 2.6 mm thick glass substrate.

Backscattering from this substrate of quanta, which had transmitted the absorber, is taken into account.

III. Measurements

The MTF of the Siemens Mammomat Novation^{DR} was measured according to the standard procedure defined in IEC 62220-1 using an edge phantom (Fig. 1) [13] or by means of a lead bar pattern (Fig. 2). Although this standard relates to radiographic detectors, we have adopted this scheme since a draft for a similar standard for mammographic detectors is in preparation. The W edge was 2 mm thick and was placed 5 cm from the chest wall side of the detector. An Al filter was located close to the tube. For the evaluations a 256×256 pixel region was used.

The anti-scatter grid was removed prior to all measurements.

Both resolution objects bring about comparable results (Fig. 3). Since the lead bar method delivers the MTF only at a few points along on the frequency axis, a smooth polygon can be drawn. The edge method results in an MTF measurement with greater uncertainty. According to the MTF definition [14], MTF values always have to be positive. Thus, strong fluctuations in the MTF lead to a rise around the point where the sinc function equals zero. The simulated curve runs slightly above the set of measured curves. This deviation is still awaiting an explanation.

To investigate the differences between measured and simulated MTF, the X-ray spectra were varied from very soft (Mo anode, 23 kV, 30 μm Mo filtration, no additional filtering object) to hard (35 kV, W anode, 50 μm Rh filtration, 2 mm Al). Although the MTF is known to be rather isotropic [10], the measurements were again carried out in horizontal, vertical, and diagonal orientation on the detector plane.

An additional problem can arise in the case of an edge phantom. With the phantom placed flat on the detector, parallax effects might occur. Therefore, the measurements were repeated with the edge slightly tilted and thus aligned towards the X-ray tube focus. As can be seen from Fig. 4, the results were the same, because the 2 mm thick tungsten edge is thick enough to easily absorb the soft mammographic radiation in every orientation of the edge phantom.

IV. Results

Fig. 5 shows the MTF curves obtained with a spectrum of a W anode, 28 kV, 50 μm Rh prefiltration, and an additional 2 mm Al filter. At low spatial frequencies (i.e., <0.5 mm^{-1}) a small drop in MTF of magnitude 2% to 3% is visible. Long-range processes deteriorating the spatial resolution cause this so-called "low-frequency drop". One phenomenon most likely to be responsible for such kind of behavior is X-ray scatter. Scattered quanta can emerge from objects between source and detector such as filters, phantoms, or the patient, but backscattering can also occur from matter behind the detector. The scattered quanta may hit any location on the detector surface and will therefore reduce the MTF over the whole spatial frequency range.

To take scattered quanta correctly into account, the simulations were performed with the edge phantom. This results in extremely long calculation times (about 100 h), because most quanta become scattered and, among these, most do not hit the detector. As a consequence of that, the resulting MTF curves look rather noisy.

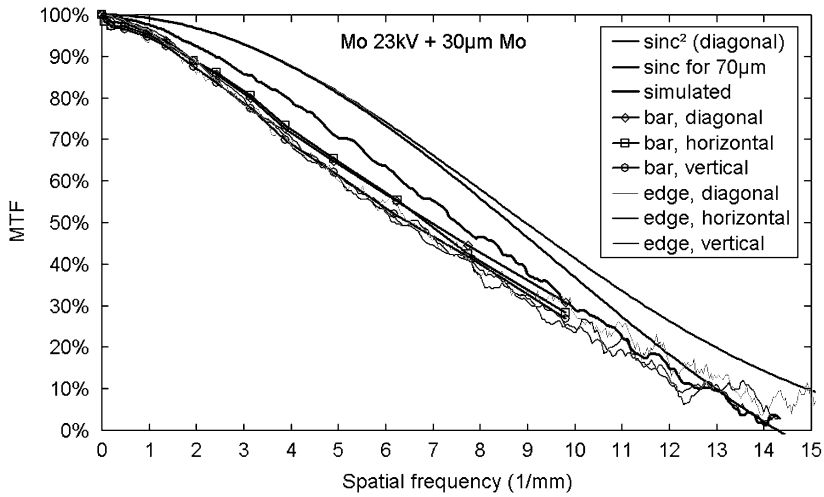

Fig. 3. MTF as a function of spatial frequency determined with a low energy mammography spectrum (Mo anode, 23 kV, 30 μm Mo prefiltration). Edge and lead bar method lead to comparable results. Further more, horizontal and vertical MTF are equal. The diagonal MTF is slightly higher, as is the theoretical limit, i.e., (4) instead of (1). The simulated curve runs slightly above the set of measured curves.

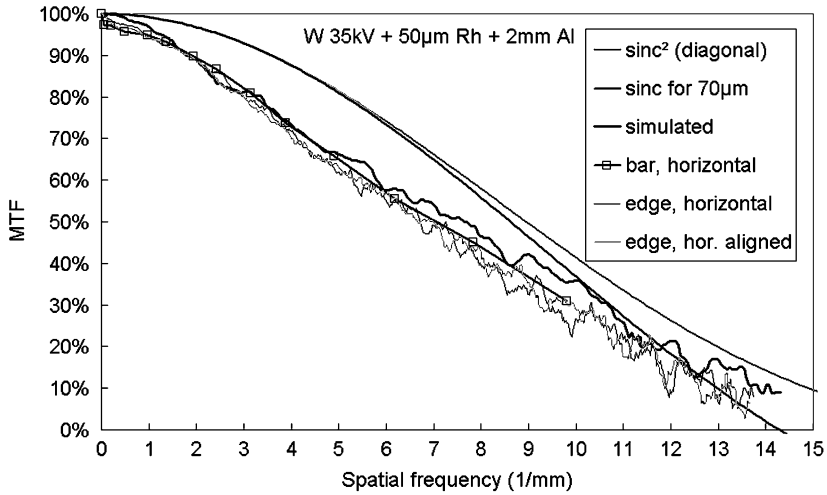

Fig. 4. MTF determined with a mammography spectrum (W anode, 35 kV, 50 μm Rh prefiltration, 2 mm Al additional filter). The edge positioned flat on the detector or aligned to the focus leads to equivalent results. The simulated MTF well agrees with the measurements.

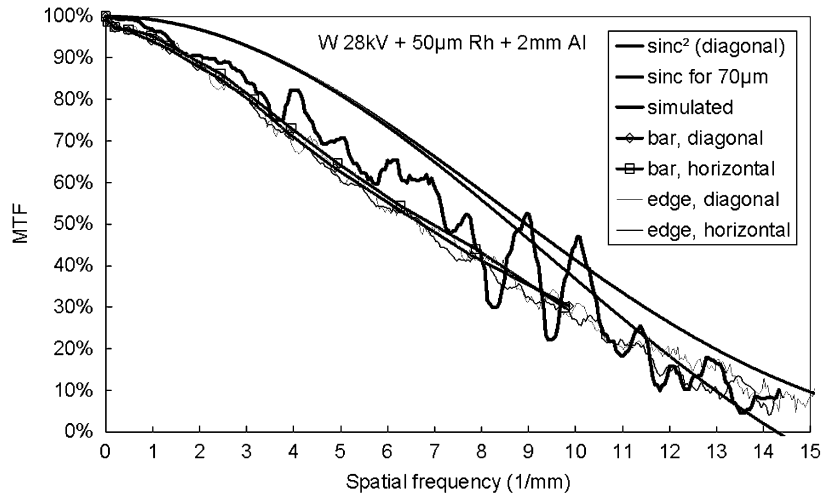

Fig. 5. MTF determined with a mammography spectrum (W anode, 28 kV, 50 μm Rh prefiltration, 2 mm Al additional filter). The low-frequency drop is 2% to 3%.

In Fig. 6, we used a 40-mm PMMA block instead of the Al sheet. The simulated as well as the measured MTF curves are displayed in comparison to the sinc function. The PMMA causes much more scatter, which leads to a strong low-frequency drop

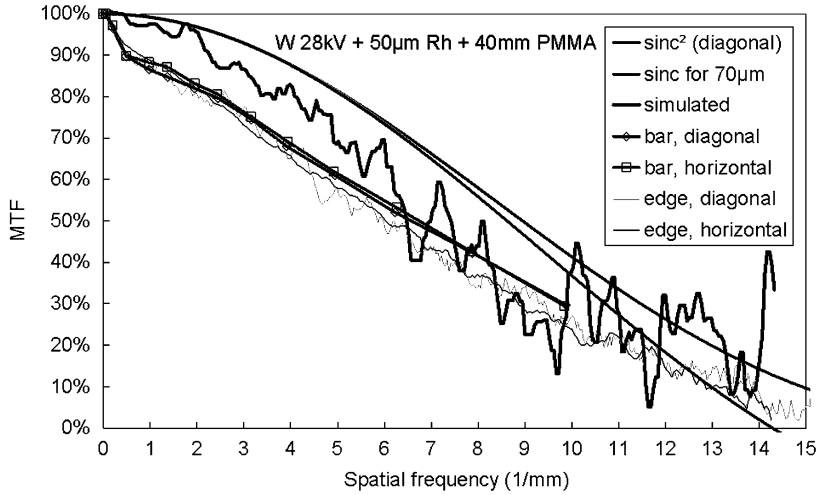

Fig. 6. MTF determined with a mammography spectrum (W anode, 28 kV, 50 μm Rh prefiltration, 40 mm PMMA additional filter). The low-frequency drop is due to scatter from the phantom and amounts to around 10%.

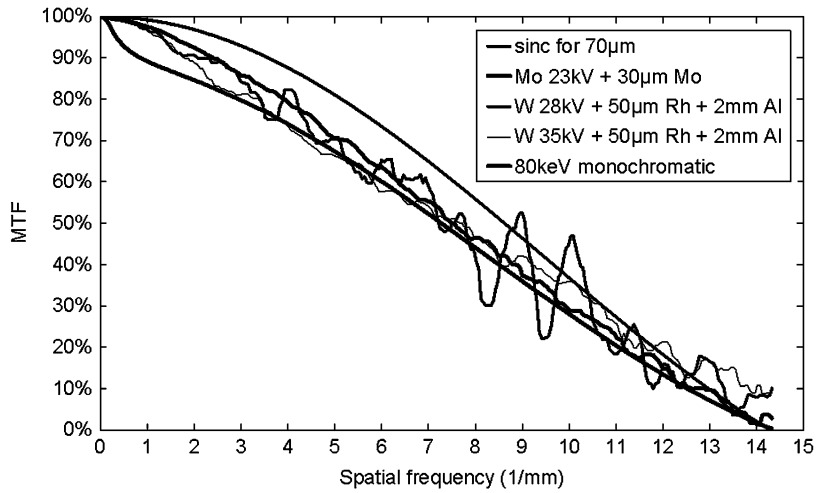

Fig. 7. Simulated MTF calculated for different mammography spectra. At higher energy (80 keV) a low-frequency drop due to backscattering from the substrate is visible.

of some 10% at 0.5 mm^{-1}. This behavior was already reported by Bätz *et al.* [15]. The Al filter, however, which is located close to the tube produces only little scatter. Moreover, since the detector is above 50 cm away from the filter the probability for scattered quanta to reach the detector is only low.

The experimentally determined MTF suffers from the fact that the phantom has to be placed on top of the object table, but the absorbing detector layer is about 2 cm below (The space is necessary to accommodate the anti-scatter grid which, however, was absent during the MTF measurements.). This allows scattered radiation to intrude in the gap between edge phantom and a-Se layer. Thus the determined MTF is lower than the MTF the detector would deliver under optimum conditions.

The simulated curves follow the overall trend given by the sinc function, but stay below it due to X-ray fluorescence. Since most of the incident X-ray spectra are at energies above the K-edge energy of Se (12.7 keV), fluorescence quanta are generated and reabsorbed up to some 100 μm away from the primary interaction location, thus reducing the MTF of the detector. Because this effect is the dominant interaction process below 50 keV, the different spectra investigated lead to similar results (Fig. 7).

An additional simulation run was performed with 80 keV monochromatic quanta. While in the mammographic energy range most of the X-rays impinging on the 250-μm thick a-Se layer are absorbed, 80 keV quanta can penetrate the absorber and may become backscattered from the substrate. This results in a pronounced low-frequency drop, as can be seen in Fig. 7.

The measured MTF curves taken with different spectra are rather similar (Fig. 8). Only the curve acquired with the PMMA filter shows a strong low-frequency drop. This tampers with the measured MTF. To avoid this effect, scatter from the filters and phantoms at least should be kept as low as possible. Without the (strongly scattering) 40 mm thick PMMA filter, a higher MTF could be obtained.

There are still some deviations between simulated and measured MTF curves (Figs. 3–6), whose origin are under investigation. Scattering from the air between X-ray tube and detector can be definitely ruled out. A possible explanation is extra-focal radiation from the X-ray tube.

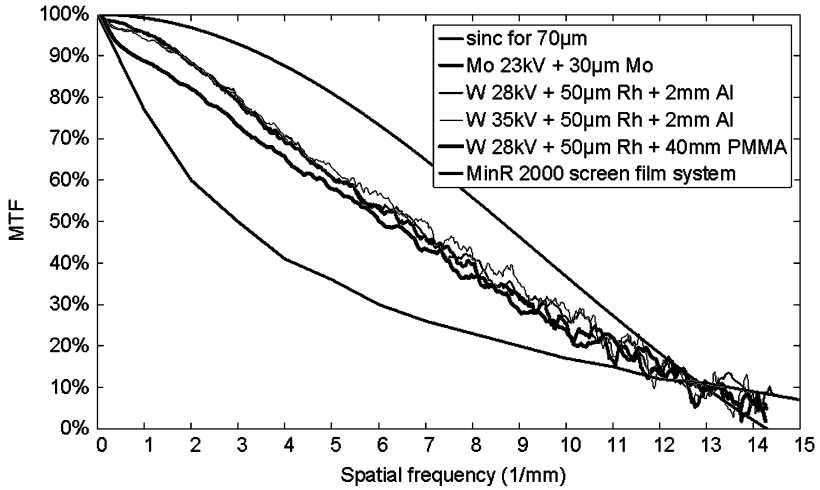

Fig. 8. Measured MTF for different mammographic spectra. PMMA filtering generates a low-frequency drop of around 10%. Data of a common film-screen system are given for comparison.

It can be expected that a-Se detector-based systems will soon replace existing film-screen systems. While films are an analog recording medium, solid-state detectors come pixelated. Fig. 8 shows that the detector under investigation with 70 μm pixels is superior in MTF over a wide spatial frequency range. The film MTF is slightly higher only beyond 13 mm^{-1}. But one has to bear in mind that the film DQE at these high frequencies is too low to be advantageous for film-screen systems [16].

V. Conclusion

The detector operation is in no way limited by the material selenium and its fundamental spatial resolution. The dominant shape of the MTF curve is given by the sinc function, i.e., it is determined by pixel aperture blur.

Moreover, the Mammomat Novation$^{\mathrm{DR}}$ by far exceeds conventional film-screen systems (e.g., Min-R) in spatial resolution, as can be seen from Fig. 8. This proves that a pixel size of 70 μm is sufficient to resolve details that are relevant for mammographic diagnosis.

Since at mammographic energies a fraction of about 90% of the X-ray energy incident on the detector is absorbed, taken together with the MTF found in this study, the prerequisites are excellent for an outstanding DQE.

Acknowledgment

The authors thank J. G. Yorker for supplying the detector data.

References

[1] J. G. Yorker, L. S. Jeromin, D. L. Y. Lee, E. F. Palecki, K. P. Golden, and Z. Jing, "Characterization of a full field digital mammography detector based on direct X-ray conversion in selenium," *Proc. SPIE*, vol. 4682, pp. 21–29, 2002.

[2] V. Loustauneau, M. Bissonnette, S. Cadieux, M. Hansroul, E. Masson, S. Savard, B. Polischuk, and M. Lehtimäki, "Image performance of a clinical selenium flat-panel detector for advanced applications in full-field digital mammography," *Proc. SPIE*, vol. 5030, pp. 1010–1020, 2003.

[3] S. Vedantham, A. Karellas, S. Suryanarayanan, D. Albagli, S. Han, E. J. Tkaczyk, C. E. Landberg, P. R. Granfors, I. Levis, C. J. D'Orsi, and R. E. Hendrick, "Full breast digital mammography with an amorphous silicon-based flat panel detector: Physical characteristics of a clinical prototype," *Med. Phys.*, vol. 27, pp. 558–567, 2000.

[4] M. M. Tesic, M. F. Piccaro, and B. Munier, "Full field digital mammography scanner," *Eur. J. Radiology*, vol. 31, pp. 2–17, 1999.

[5] D. Hoeschen and W. Mirande, "Messung der Modulationsübertragungsfunktion von Film-Folien-Kombinationen mit einem Bleiraster," *Fortschritte auf dem Gebiet der Röntgenstrahlung*, vol. 140, pp. 600–604, 1984.

[6] K. Stierstorfer and M. Spahn, "Self-normalizing method to measure the detective quantum efficiency of a wide range of X-ray detectors," *Med. Phys.*, vol. 26, pp. 1312–1319, 1999.

[7] E. Samei, M. J. Flynn, and D. A. Reimann, "A method for measuring the presampled MTF of a digital radiographic system using an edge test device," *Med. Phys.*, vol. 25, pp. 102–113, 1998.

[8] E. Buhr, S. Günther-Kohfahl, and U. Neitzel, "Accuracy of a simple method for deriving the presampled modulation transfer function of a radiographic system from an edge image," *Med. Phys.*, vol. 30, pp. 2323–2331, 2003.

[9] M. Flynn, S. Wildermann, and J. Kanicki, "The effect of secondary radiations on the performance of digital radiographic detectors," *Proceedings of the SPIE*, vol. 3336, pp. 326–336, 1998.

[10] M. Hoheisel, J. Giersch, M. Mitschke, and P. Bernhardt, "Absorbers for medical X-ray detectors with optimum spatial resolution: a simulation study," *Proc. SPIE*, vol. 5368, pp. 386–395, 2004.

[11] J. Giersch, A. Weidemann, and G. Anton, "ROSI—An object-oriented and parallel-computing Monte Carlo simulation for X-ray imaging," *Nuclear Instruments and Methods in Physics Research A*, vol. 509, pp. 151–156, 2003.

[12] K. A. Fetterly, N. J. Hangiandreou, B. A. Schueler, and E. R. Ritenour, "Measurement of the presampled two-dimensional modulation transfer function of digital imaging systems," *Med. Phys.*, vol. 29, pp. 913–921, 2002.

[13] E. Samei, E. Buhr, P. Granfors, D. Vandenbroucke, and X. Wang, "Comparison of edge analysis techniques for the determination of the MTF of digital radiographic systems," *Phys. Med. Bio.*, vol. 50, pp. 3613–3625, 2005.

[14] H. H. Barrett and W. Swindell, *Radiological Imaging—The theory of image formation, detection, and processing*. New York: Academic Press, 1981.

[15] L. Bätz, J. Eser, and T. Mertelmeier, "Detector performance of the new Siemens FFDM system," in *7th Int. Workshop on Digital Mammography*, Durham, NC, 2004.

[16] P. C. Bunch, "Objective imaging characteristics of mammographic screen-film systems," *Proc. SPIE*, vol. 2708, pp. 241–271, 1996.